Journal of Molecular Structure 695–696 (2004) 155–162

Collisional dynamics of the first excited states of neon in the 590-670 nm region using laser optogalvanic spectroscopy

X.L. Han[a], M.C. Su[b], C. Haridass[c], P. Misra[d,*]

[a]*Department of Physics and Astronomy, Butler University, Indianapolis, IN 46208, USA*
[b]*Department of Chemistry, Butler University, Indianapolis, IN 46208, USA*
[c]*Department of Physical Sciences, Belfry School, Belfry, KY 41514, USA*
[d]*Laser Spectroscopy Laboratory, Department of Physics and Astronomy, Howard University, Washington, DC 20059, USA*

Received 1 October 2003; accepted 4 November 2003

ELSEVIER

2004

Available online at www.sciencedirect.com
SCIENCE DIRECT®
Journal of Molecular Structure 695–696 (2004) 155–162
Journal of MOLECULAR STRUCTURE
www.elsevier.com/locate/molstruc

Collisional dynamics of the first excited states of neon in the 590-670 nm region using laser optogalvanic spectroscopy

X.L. Han[a], M.C. Su[b], C. Haridass[c], P. Misra[d,*]

[a]*Department of Physics and Astronomy, Butler University, Indianapolis, IN 46208, USA*
[b]*Department of Chemistry, Butler University, Indianapolis, IN 46208, USA*
[c]*Department of Physical Sciences, Belfry School, Belfry, KY 41514, USA*
[d]*Laser Spectroscopy Laboratory, Department of Physics and Astronomy, Howard University, Washington, DC 20059, USA*

Received 1 October 2003; accepted 4 November 2003

Abstract

A mathematical rate equation model, incorporating the various processes contributing to the generation of optogalvanic signals in a discharge plasma, has been used to analyze the time-resolved waveforms of neon in the wavelength region 590–670 nm. Amplitudes, decay rates and the appropriate instrumental time constant have been determined using a non-linear least-squares fit of the observed time-resolved optogalvanic waveforms.

Keywords: Collisional dynamics; Neon transitions; Optogalvanic spectroscopy; Decay rates; Time-dependent waveforms

1. Introduction

Laser optogalvanic spectroscopy is a sensitive and selective technique that can be used in a variety of spectroscopic investigations, including plasma diagnostics and analytical flame spectroscopy. Optogalvanic (OG) detection is primarily accomplished by measuring the effects of either a change in impedance or a variation in current in a discharge or a flame environment. OG transitions have been observed for various species sputtered from hollow cathodes and from gas-discharge flash lamps filled with inert gases, especially neon and argon. Gusev and Kompanets [1] pointed out the difficulty in obtaining OG resonances with neon at wavelengths shorter than 580 nm because of low oscillator strengths of such resonances. Zhu et al. [2], however, observed laser-assisted OG signals with neon in the 337–598 nm region by employing a commercial ion–neon hollow cathode lamp (HCL). In this study, the authors identified 223 OG transitions to be associated with neon energy levels and surprisingly found that there were more neon OG lines in the near-UV region than in the yellow and red regions and that these transitions were fairly intense. OG transitions of argon have also been observed in the UV and visible regions. Over the years numerous investigations have been carried out on the observation of the OG lines for neon extending from the UV to the red spectral region. For the earlier work on the OG lines of neon, the reader is referred to Barbierri et al. [3] and Haridass et al. [4]. Ullas et al. [5] used a helium–neon laser and an Ar^+ laser pumped dye laser to study OG double resonance spectra of neon. The double resonance signals were identified via two-step excitation involving the same or different intermediate levels. These authors also studied the variation of the OG signals with laser power, discharge voltage, current and chopping frequencies [5]. Narayanan et al. [6] observed 45 lines in the OG spectra of neon in the region 610–730 nm using a Nd-YAG -pumped dye laser and a Fe–Ne HCL. The origins of these lines were from one and two photon transitions in the neon atom. Kumar et al. [7] observed and assigned 440 lines in the spectral region 410–545 nm using a Fe–Ne HCL and an excimer laser-pumped dye laser.

The work cited above for neon record OG intensities in various UV-visible wavelength domains. In addition, there are other studies [3,4,8,9] reported in the literature that identify and quantitatively characterize the dominant physical processes contributing to the production of OG

* Corresponding author. Tel.: 1-202-806-4913; fax: 1-202-806-4429.
E-mail address: pmisra@howard.edu (P. Misra).

0022-2860/$ - see front matter © 2004 Elsevier B.V. All rights reserved.
doi:10.1016/j.molstruc.2003.11.044

signals in a discharge plasma. Stewart et al. [9] developed a theoretical model to study the 640.2 nm ($1s_5-2p_9$) transition using the ground-state atom and electron collisional mixing of both the 1*s and 2p states. The rate-equation model used a large number of parameters (~150) and provided remarkable agreement between theory and experiment for the discharges at two pressures (1.5 and 2.0 Torr), but failed at higher pressures. Han et al. [8] used a simple mathematical rate equation model (with 4 parameters) involving decay rates and collisional ionization efficiencies for the states involved and produced a good simulation of the observed OG waveforms for the 640.2 nm ($1s_5-2p_9$) transition at different (2–14 mA) currents.

Electron heating effects can become very important in the case of the hollow cathode discharge when the atoms sputtered from the cathode are excited by laser radiation. Keller et al. [10] performed a calculation, using a standard model of the hollow cathode discharge, which showed that the OG generation mechanism involving direct collisional energy transfer from absorbing atoms to electrons was approximately 100 times more effective than direct ionization for a laser-excited level. Such an effect can be explained by assuming that the atomic system simply transfers the excitation energy to the electrons. Normally, owing to the presence of elastic and super elastic collisions between the electrons and the atoms, the electron temperature established in a hollow cathode approximately equals the electronic excitation temperature of the atom, which in turn gets slightly perturbed by the laser radiation. The electron collisions are so frequent that a significant change in the level population is prevented, however, and the energy supplied by the absorbed photons is transferred to the electrons. Since the equilibrium in the discharge is strongly affected by the electron energy distribution, such extra energy brings about a decrease or increase in the impedance of the discharge.

In the present study, we use a mathematical rate equation model that represents the processes contributing to the production of the OG signal in a discharge plasma, namely electron collisional excitation, radiative depopulation, electron collisional ionization and collisional redistribution to analyze the time-resolved OG waveforms of neon in the region 590–670 nm. Amplitudes, decay rates and the instrumental time constant have been obtained by fitting the observed time resolved OG waveforms with a non-linear least squares fit program.

2. Experimental

The experimental arrangement used for recording the OG spectra is shown in Fig. 1. In this figure, a home-built dye laser is pumped by the second harmonic of a Continuum Nd: YAG-laser (Model Surelite) running at 10 Hz. The output beam had a pulse duration of about 5–7 ns and a nominal line width of 0.07 cm^{-1}. The tuning range in the visible region was covered by several laser dyes. A series of optics (an aperture, two lenses, a mirror and a beam splitter) are inserted in the optical path of the laser beam. A pair of lenses are placed several centimeters apart to collimate the beam at the reaction point inside the HCL. The beam spliter is used for guiding the light to a photodiode and to eliminate the unresolved pump beam in the UV region of the dye laser. One of the beams entered a magnesium HCL (Perkin Elmer) filled with approximately 6–8 Torr of neon gas. The HCL

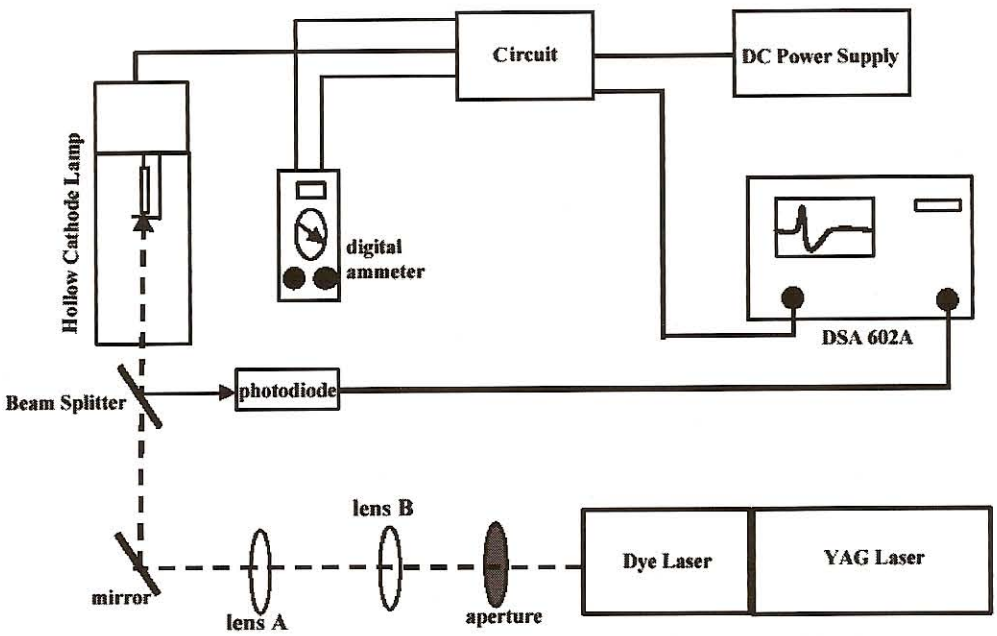

Fig. 1. Schematic experimental arrangement for laser Optogalvanic Spectroscopy.

was coupled in series with a current-limiting RC circuit, where R and C are 2.2 kΩ and 0.01 μF, respectively.

The discharge current was continuously adjustable within the lamp's working range. The second beam from the beam splitter is directed to the photodiode in order to trigger the scope DSA602A. The DSA602A is set to average either 256 or 512 OG signals, depending on the quality of the signals. A complete data set consists of a total of 16 spectra for a specific transition involving data acquisition for 7 mA to 14 mA discharge currents, and back to 7 mA, at an increment of 1.0 mA. The stored data from the scope is converted to DOS text format and further analyses performed using a non-linear least squares fit program.

3. Theoretical model

Lawler [11] modeled the OG effect in the positive column in terms of a perturbed rate equation that included dynamic impedance, and his theoretical model provided excellent agreement with the experimental observations for helium gas. Later, Doughty and Lawler [12] extended this model to neon in the visible region and again obtained good agreement with a simplified description of the complex energy level system. The improved theoretical understanding of the OG effect in a variety of environments has made it an important quantitative diagnostic technique. As different models have progressed from a simple structure to a more comprehensive inclusion of important discharge processes, it is apparent that some of the descriptions in the models did not agree well with the experimental observations. Such discrepancies led Stewart et al. [9] to develop a model that included and identified specifically and quantitatively the dominant effects of electron collisional transfer and resonance wall losses. The authors included separate rate equations for neon atoms involving all four 1s states and discussed the agreement of the model with the measured OG signals for a number of transitions in the visible region, involving $1s_4$ and $1s_5$ states, and also over a wide range of discharge pressures and currents. Subsequently, Han et al. [8] used a theoretical model involving only few parameters (four), and studied the OG effect associated with the signal of neon that Stewart et al. [9] had analyzed earlier, and clearly identified and quantitatively characterized the dominant physical processes that contributed to the production of the OG signal. Since the theory of dominant physical processes in discharges is well documented in the literature [4,8], salient features of the model (Fig. 2) will be discussed in the present work. Prior to laser excitation, there exists a state of dynamical equilibrium in the atomic distribution in each energy level. Upon laser excitation from $|L_1>$ to $|L_2>$, a fraction of the excited buffer gas atoms are collisionally transferred from $|L_2>$ to other $|L_2'>$ states and then they radiatively decay back to the $|L_n>$ states (where n =3,4 and 5) within the radiative lifetime of the $|L_2>$ state. The subsequent population change over time (as illustrated in Fig. 2) for all the states can be expressed as

$$\frac{dN_{L1}}{dt} = R_{L1} - N_{L1}(\Gamma_{L1} + IP_{L1} + IP_{L1s}) \quad (1)$$

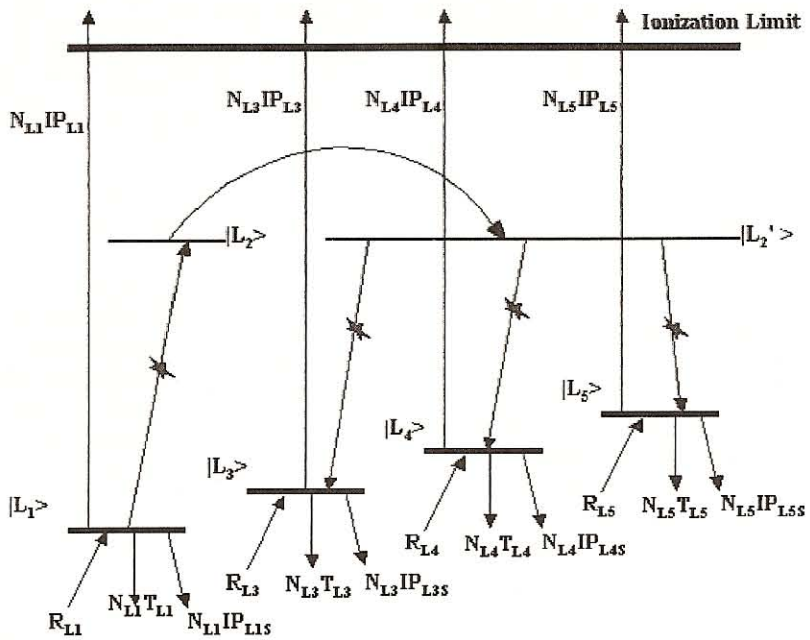

Fig. 2. Four-level energy diagram illustrating the dynamics involved in the generation of the optogalvanic signal (*indicates laser excitation and radiative decays). In the present investigation of the neon 1s–2p transitions $|L_1>$, $|L_3>$, $|L_4>$ and $|1L_5>$ represents $|1s_2>, |1s_3>, |1s_4>, |1s_5>$ levels, respectively, and $|L_2>$ represents the p (p1–p10) levels. In case of the neon $1s_5$–$2p_9$ transition, $|L_1>$ represents the $|1s_5>$ level and $|L_2>$ represents the $|2p_9>$ level. Here $|L_2'>$ represents other p levels.

$$\frac{dN_{L3}}{dt} = R_{L3} - N_{L3}(\Gamma_{L3} + IP_{L3} + IP_{L3s}) \quad (2)$$

$$\frac{dN_{L4}}{dt} = R_{L4} - N_{L4}(\Gamma_{L4} + IP_{L4} + IP_{L4s}) \quad (3)$$

$$\frac{dN_{L5}}{dt} = R_{L5} - N_{L5}(\Gamma_{L5} + IP_{L5} + IP_{L5s}) \quad (4)$$

where R_{L1}, R_{L3}, R_{L4} and R_{L5} are the rate constants for collisional excitation of the states $|L_1>$, $|L_3>$, $|L_4>$ and $|L_5>$, respectively, from all of the lower states. N_{Li} and Γ_{Li} are, respectively, the neon population and effective decay rates of the $|L_i>$ states. IP_{Li} is the total probability of ionization of the state $|L_i>$, I is the current, and P_{Li} is related to the collisional ionization cross section of the $|L_i>$ state.

The OG signal (w(t)) due to ionization of $|L_1>$ and other $|L_i>$ states can be expressed as

$$\begin{aligned}\Delta w(t) &= \Delta N_{L1} IPL_1 + \Delta N L_3 IPL_3 + \Delta N L_4 IPL_4 + \Delta N L_5 IPL_5 \\ &= \Delta N_0 \{IP_{L3} e^{[-(\Gamma_{L3}+IP_{L3}+IP_{L3s})t]} - IP_{L1} e^{[-(\Gamma_{L1}+IP_{L1}+IP_{L1s})t]} \\ &\quad + IP_{L4} e^{[-(\Gamma_{L4}+IP_{L4}+IP_{L4s})t]} + IP_{L5} e^{[-(\Gamma_{L5}+IP_{L5}+IP_{L5s})t]}\}\end{aligned} \quad (5)$$

Eq. (5) is recognized as a form composed of four exponential decays associated with the $|L_1>$, $|L_3>$, $|L_4>$ and $|L_5>$ states, and yields the experimental time resolved OG signal as

$$w(t) = \frac{\Delta w(t)}{\Delta N_0} = a e^{-bt} - c e^{-dt} + e e^{-ft} + g e^{-ht} \quad (6)$$

where

$$\begin{aligned}&a = IPL_3, b = \Gamma_{L3} + I(PL_3 + PL_{3s}); c = IP_{L1}, d = \Gamma_{L1} \\ &\quad + I(P_{L1} + P_{L1s}); e = IP_{L4}, \quad f = \Gamma_{L4} + I(P_{L4} + PL_{4s}); \\ &g = IP_{L5}, h = \Gamma_{L5} + I(P_{L5} + PL_{5s})\end{aligned} \quad (7)$$

By varying the discharge current, and therefore changing the evolution rate, we can compile a set of time-resolved OG waveforms in order to reveal the effects of varying the discharge currents. Based on the theoretical model described above, each spectrum is fitted using a non-linear least-squares method in order to obtain the parameters associated with the optical energy states. The effect of the instrumental time constant (τ) is crucial in determining the fast time region of the OG waveform and can only be determined experimentally [13,14]. The instrumental response becomes less significant as the OG signal evolves in the time domain. When the instrumental time constant is included in Eq. (6), the expression for the experimental time resolved OG signal (s(t)) can be written as

$$\begin{aligned}s(t) &= \frac{a}{1-b\tau}\left[e^{-bt} - e^{-\left(\frac{t}{\tau}\right)}\right] - \frac{c}{1-d\tau}\left[e^{-dt} - e^{-\left(\frac{t}{\tau}\right)}\right] \\ &\quad + \frac{e}{1-f\tau}\left[e^{-ft} - e^{-\left(\frac{t}{\tau}\right)}\right] + \frac{g}{1-h\tau} \\ &\quad \times \left[e^{-ht} - e^{-\left(\frac{t}{\tau}\right)}\right]\end{aligned} \quad (8)$$

where a, c, e and g are the positive, negative, positive and positive amplitudes, respectively, and b, d, f and h are proportional to the decay rates of the s state. τ is the instrumental time constant.

4. Results and discussion

Kane [15] has studied the ionization mechanism of the $1s_5-2p_2$ transition of the neon atom and explored the effects of various ionization conditions under different laser powers and also the location of the OG effect between the electrodes. This author also recorded the emission lines arising from the excited p state. Kane's study implied that the disruption in the steady state among the available 1s states induced a variation in ionization and thus caused the OG signals to be observed. Veldhuizen et al. [16] investigated the time-resolved OG waveform for the same transition. Preliminary experiments conducted by Wisehart [17] suggested that there might be a correlation between the initial state of the atomic transition and the polarity of the OG signals. Most of the work cited in the literature has focused often on one or two specific transitions and the associated OG effect. A complete understanding of the collisional dynamics (decay rates, polarity of the signal, collisional cross-sections) involving all the levels of the 1s state is not yet well understood. This prompted us to record the time-resolved waveforms of neon transitions involving 1s states (as their initial states) and thereby attempt to identify and qualitatively characterize the dominant physical processes contributing to the production of the OG signals.

For the neon 1s–2p transition, employing the Paschen notation, there are four 1s states and ten 2p states, which yield a total of 30 allowed radiative transitions. A schematic representation of the 30 allowed transitions for the neon atom between the s and p states, along with their corresponding wavelengths (Å), is given in Fig. 3. Of the four 1s states, two ($1s_3$ and $1s_5$) are metastable with radiative life times of the order of 1s, while the other two ($1s_2$ and $1s_5$) decay to the ground state within 1 ns. In the present work, we have chosen five different transitions, namely: $1s_2-2p_4$: 667.8276 nm, $1s_3-2p_2$: 616.3594 nm, $1s_4-2p_6$: 630.4789 nm, $1s_5-2p_4$: 594.4834 nm and $1s_5-2p_9$: 640.2246 nm, in order to determine the rate constants of the initial state and the optically allowed

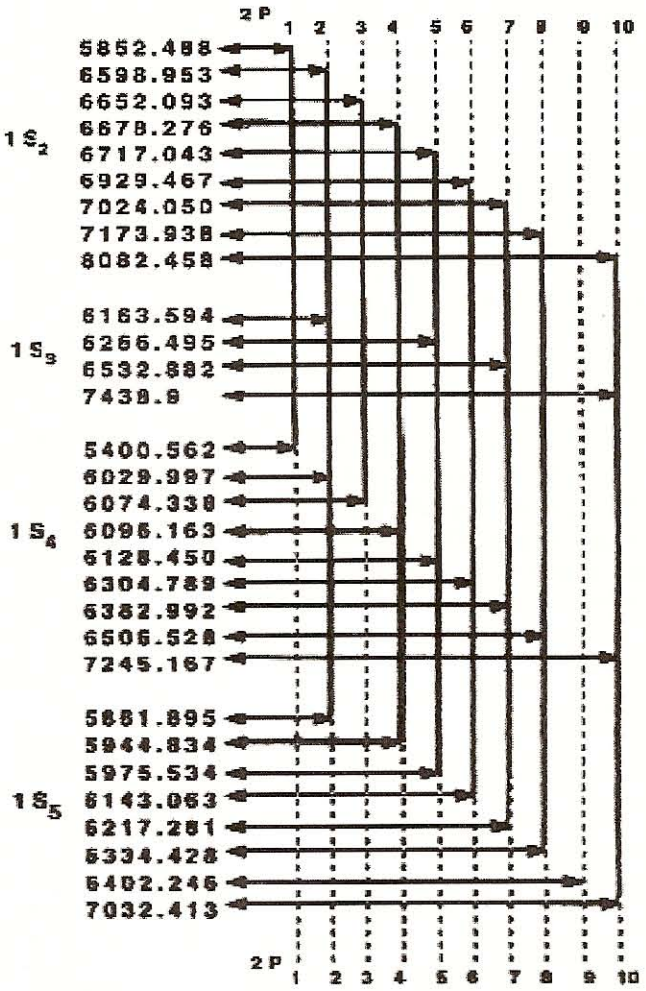

Fig. 3. Schematic representation of the allowed transitions of the neon atoms between the 1s–2p (Paschen notation) states, along with their corresponding wavelengths (Å).

decaying states. These transitions have been recorded at various currents: 7–14 mA, and back to 7 mA, at increments of 1 mA, and a complete set of data for each transition comprises of 16 spectra. A typical observed OG waveform of the Ne-transition ($1s_5$–$2p_4$) at 594.4834 nm for discharge currents 7–14 mA is shown in Fig. 4. The waveforms were fitted to Eq. (8) by using a non-linear least squares fit program. For each transition, the amplitude, rate constant and the instrumental time constant were determined. Let us consider each individual transition in turn and attempt to understand the process involved in re-creating the time-resolved OG waveforms.

$1s_5$–$2p_4$ transition: Of the 30 allowed transitions shown in Fig. 3, we have chosen this transition at 594.4834 nm because laser excitation from the $1s_5$ to the $2p_4$ state results in the excited neon atoms relaxing to the optically allowed $1s_4$ and $1s_2$ states. By analyzing the associated waveform, it is possible to obtain the decay rates for the $1s_5$, $1s_4$ and the $1s_2$ states, as well as the positive and negative amplitudes and the instrumental time constant.

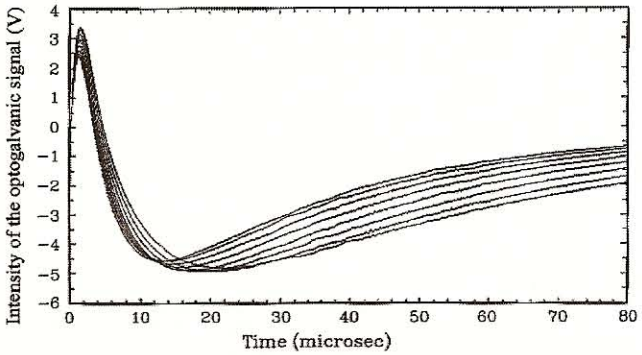

Fig. 4. Observed optogalvanic waveforms of the neon transition ($1s_5$–$2p_4$) at 594.4834 nm for eight (7–14 mA) different currents.

The observed time-resolved OG waveforms for 8 different (7–14 mA) currents are shown in Fig. 4. According to the above mentioned scheme, the observed waveform can be fitted to the expression in Eq. (8) involving only the first three terms:

$$s(t)\frac{a}{1-b\tau}\left[e^{-bt}-e^{-\left(\frac{t}{\tau}\right)}\right]-\frac{c}{1-d\tau}\left[e^{-dt}-e^{-\left(\frac{t}{\tau}\right)}\right]+\frac{e}{1-f\tau}\left[e^{-ft}-e^{-\left(\frac{t}{\tau}\right)}\right] \quad (9)$$

where a, c and e are the positive, negative and positive amplitudes, respectively; and b, d and f are the decay rates for the states involved in the transition, respectively. τ is the instrumental time constant of the waveform representing the OG signal. Although, in principle, one can include all the four terms to fit the observed OG signal, in the present work, for this particular transition, we were able to use only the first two terms in Eq. (9) to fit the observed neon OG waveforms satisfactorily for all of the eight (7–14 mA) currents. A non-linear least-squares program was used. The observed and fitted time-resolved OG waveforms for one particular current 10 mA are shown in Fig. 5. The values of the fitted constants are given in Table 1.

After the neon atoms are excited from the $1s_5$ to the $2p_4$ state, the atom quickly decays to all available radiatively coupled states namely $1s_4$ and $1s_2$ states. In the fit, the parameter d is set so that it represents the total decaying rate of the initial state ($1s_5$) upon excitation to the $2p_4$ state. This is evidenced by the negative amplitude c associated with the exponential function given in Eq. (9). Thus, the value of the decay rate d corresponds to the initial state, which is the $1s_5$ state. The decay rate b obtained may belong to either the $1s_4$ or the $1s_2$ state.

$1s_5$–$2p_9$ transition: In order to check the consistency and accuracy of the decay rates for the $1s_5$ state and our overall analysis, we chose the neon transition $1s_5$–$2p_9$ at 640.2246 nm, which has the same initial state as the previous transition $1s_5$–$2p_4$. The observed time-resolved OG waveforms for 8 different (7–14 mA) currents were

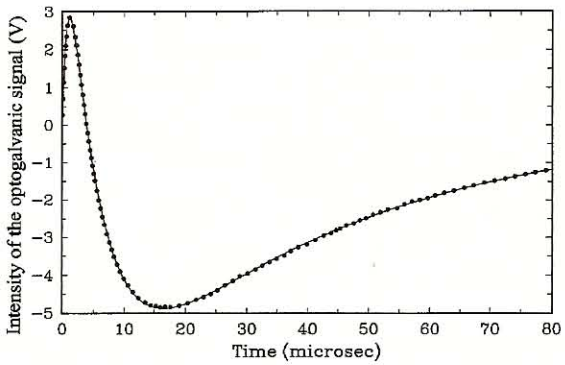

Fig. 5. Fitted and observed optogalvanic waveforms of the neon transition ($1s_5$–$2p_4$) at 594.4834 nm for 10 mA current. Dotted line corresponds to the experimental waveform and the solid line corresponds to the fitted waveform.

fitted to Eq. (9) involving only two exponential terms. The decay parameters b and d thus obtained from the fit are given in Table. 2

It is very clear from Table 2 that the decay rate constant (d) for the $1s_5$ state for this transition is in agreement with the value obtained from a different transition having the same initial state, which in turn confirms that our data and analysis are consistent and reliable.

$1s_3$–$2p_2$ transition: Of the 30 allowed neon transitions shown in Fig. 3, we have chosen this transition at

Table 1
Fitted decay rates obtained from a non-linear least-squares fit of the observed optogalvanic waveforms for neon at 594.4834 nm for eight currents (7–14 mA)

Current (mA)	b (μs^{-1})	d (μs^{-1})
7	0.159	0.021
8	0.157	0.020
9	0.171	0.022
10	0.187	0.024
11	0.203	0.026
12	0.220	0.029
13	0.238	0.030
14	0.254	0.031

Table 2
Fitted decay rates obtained from a non-linear least-squares fit of the observed optogalvanic waveforms for neon at 640.2246 nm for eight currents (7–14 mA)

Current (mA)	b (μs^{-1})	d (μs^{-1})
7	0.102	0.025
8	0.124	0.024
9	0.133	0.026
10	0.159	0.027
11	0.183	0.027
12	0.197	0.032
13	0.223	0.032
14	0.241	0.034

Table 3
Fitted decay rates obtained from a non-linear least-squares fit of the observed optogalvanic waveforms for neon at 616.3594 nm for eight currents (7–14 mA)

Current (mA)	b (μs^{-1})	d (μs^{-1})
7	0.118	0.037
8	0.116	0.038
9	0.114	0.039
10	0.112	0.040
11	0.107	0.043
12	0.113	0.042
13	0.114	0.043
14	0.116	0.043

616.3594 nm, because following laser excitation from the $1s_3$ to the $2p_2$ state, the excited neon atoms are able to relax to optically allowed $1s_5$, $1s_4$ and $1s_2$ states. By analyzing the associated waveforms, it is possible to determine the decay rates for the $1s_5$, $1s_4$ and $1s_2$ states. The observed time-resolved OG waveforms for eight different (7–14 mA) currents were fitted to Eq. (9). The decay rate constants b and d thus obtained from the fit are given in Table 3.

The decay rate (d) for the $1s_3$ state is very close to the value for the $1s_5$ state. This is probably true because both are metastable states of the neon atom. The values of the decay rate (b) so obtained from the present fit could not be assigned to the $1s_5$ state because these values are somewhat different from those obtained earlier and summarized in Tables 1 and 2. The decay rates (b) obtained in the present work may be attributed to the $1s_4$ state.

$1s_4$–$2p_6$ transition: This particular transition exists around 630.4789 nm, where the neon atoms after excitation can relax back to three states, namely $1s_2$, $1s_4$ and $1s_5$. The observed time-resolved OG waveforms for eight different (7–14 mA) currents are shown in Fig. 6. According to the above mentioned scheme, the observed waveforms can be fitted to the expression in Eq. (8) involving

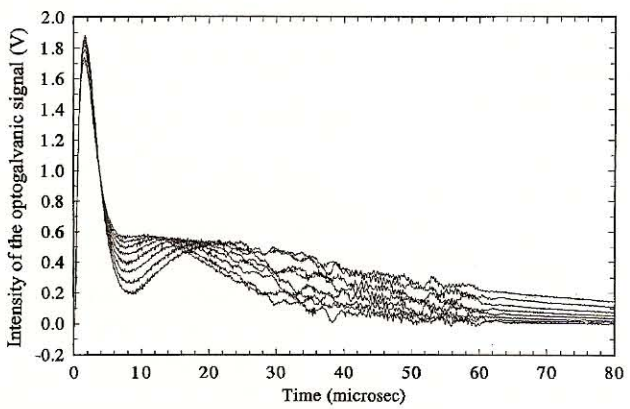

Fig. 6. Observed optogalvanic waveforms of the neon transition ($1s_4$–$2p_6$) at 630.4789 nm for 8 different (7–14 mA) currents.

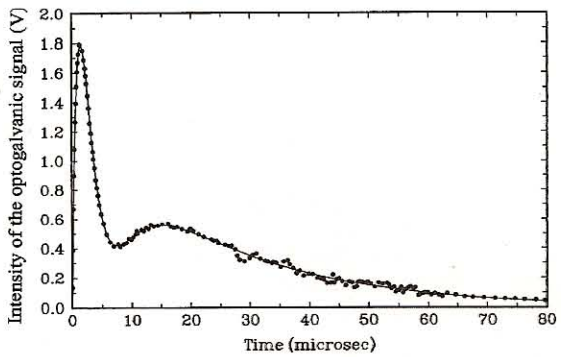

Fig. 7. Fitted and observed optogalvanic waveforms of the neon transition ($1s_4$–$2p_6$) at 630.4789 nm for 10 mA current. Dotted line corresponds to the experimental waveform and the solid line corresponds to the fitted waveform.

the first three terms:

$$s(t)=\frac{a}{1-b\tau}\left[e^{-bt}-e^{-\left(\frac{t}{\tau}\right)}\right]-\frac{c}{1-d\tau}\times\left[e^{-dt}-e^{-\left(\frac{t}{\tau}\right)}\right]+\frac{e}{1-f\tau}\left[e^{-ft}-e^{-\left(\frac{t}{\tau}\right)}\right] \quad (10)$$

where a, c and e are the positive, negative and positive amplitudes, respectively; and b, d and f are the decay constants. A non-linear least-squares program was used again to fit Eq. (10). The observed and fitted time-resolved OG waveforms for one particular current 10 mA are shown in Fig. 7. The values of the fitted constants are given in Table 4. The decay rate (d) for the $1s_4$ state was found to be roughly two times larger than the value observed for the decay constant (b) obtained in Table 3. The values for the decay rates b and f correspond to the $1s_2$ and $1s_5$ states. We attempted to obtain the OG signals for the $1s_2$–$2p_4$ transition at 667.8276 nm. As noted earlier, the rate constants are relatively large for the $1s_2$ state, whereby it was very difficult to record these OG signals for different currents. A plot of the decay rate constants versus the current (as illustrated in Fig. 8) shows interesting

Table 4
Fitted decay rates obtained from a non-linear least-squares fit of the observed optogalvanic waveforms for neon at 630.4789 nm for the currents 7–14 mA

Current (mA)	τ (μs)	a (V)	b (μs^{-1})	c (V)	D (μs^{-1})	e (V)	f (μs^{-1})
7	1.27	7.43	0.433	−4.11	0.196	1.00	0.0257
8	1.27	7.52	0.452	−4.24	0.210	1.10	0.0310
9	1.35	8.17	0.493	−4.68	0.250	1.12	0.0367
10	1.37	8.43	0.522	−4.91	0.273	1.20	0.0428
11	1.35	8.43	0.537	−5.09	0.285	1.35	0.0516
12	1.37	8.63	0.564	−5.34	0.304	1.49	0.0610
13	1.32	8.61	0.570	−5.67	0.318	1.62	0.0718
14	1.22	8.28	0.556	−5.87	0.315	1.90	0.0826

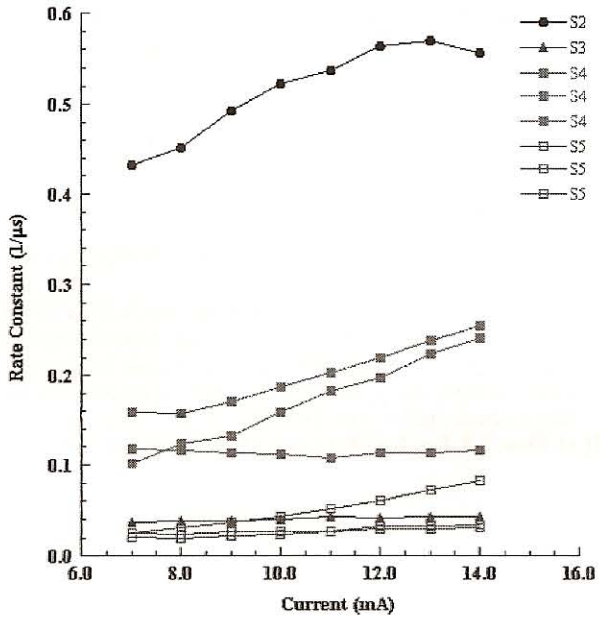

Fig. 8. A plot of the rate constant versus current for the optogalvanic neon transitions associated with the states $1s_2$, $1s_3$, $1s_4$ and $1s_5$.

characteristics pertaining to all the 1 s levels associated with the neon transitions. Based on the present work, it is clear that both $1s_3$ and $1s_5$ states have almost the same rate constants owing to their metastable nature. All of the rate constants show a predominantly linear variation with increasing current. The decay rate found for the $1s_2$ state is of higher value than all the other 1s states.

5. Conclusion

In the present work, based on a comprehensive rate equation model, we have been able to use the recorded time-resolved OG waveforms and identify the dominant discharge process-namely, the electron collisional ionization of neon, to be responsible for the OG signals generated in the wavelength region 590–670 nm. We have selectively identified and studied specific OG transitions that have yielded a wealth of information relating to the decay rates of all the 1s levels involved either directly or indirectly in these transitions. A strong indication of state dependence of the investigated OG signals was also observed.

Acknowledgements

Financial support from the Research Corporation and the NASA-funded Center for the Study of Terrestrial and Extraterrestrial Atmospheres is gratefully acknowledged.

The authors deeply appreciate Mr Girum Gugsa's technical help in preparing the final manuscript for publication.

References

[1] V.M. Gusev, O.N. Kompanets, Sov. J. Quantum Electron 1515 (1979) 17.
[2] X. Zhu, A.H. Nur, P. Misra, J. Quant. Spectrosc. Radiat. Transfer 167 (1994) 52.
[3] B. Barbieri, N. Beverini, A. Sasso, Rev. Mod. Phys. 62 (3) (1990) 612.
[4] C. Haridass, H. Major, P. Misra, X.L. Han, Laser Optogalvanic Spectroscopy of Discharge Plasmas in the Ultraviolet Region, in Ultraviolet Spectroscopy and UV Lasers, in: P. Misra, M.A. Dubinskii (Eds.), Marcel Dekker, New York, 2002, p. 33.
[5] G. Ullas, S.B. Rai, D.K. Rai, Chem. Phys. Letters 102 (1991) 18.
[6] K. Narayanan, G. Ullas, S.B. Rai, Chem. Phys. Letters 55 (1989) 156.
[7] M. Kumar, G. Ullas, S.B. Rai, Physica Scripta 676 (1997) 55.
[8] X.L. Han, V. Wisehart, S.E. Conner, M.-C. Su, D.L. Monts, Contrib. Plasma. Phys. 439 (1995) 34.
[9] R.S. Stewart, K.I. Hamad, K.W. McKnight, In: R.S. Stewart, J. E. Lawler, Eds. Optogalvanic Spectroscopy. Inst. Phys. Conf. Ser. No. 113, Bristol, U. K: Institute of Physics, 89 (1990).
[10] R.A. Keller, R. Engleman Jr., B.A. Palmer, Appl. Opt. 863 (1980) 19.
[11] J.E. Lawler, Phys. Rev. A 1025 (1980) 22.
[12] D.K. Doughty, J.E. Lawler, Phys. Rev. A 773 (1983) 28.
[13] R. Shuker, A. Ben-Amar, G. Erez, J. Phys, (Paris) C7 (1983) 35.
[14] D.H. Dieke, H.M. Crosswhite, J. Quant. Spectrosc. Radiat. Transfer 97 (1961) 2.
[15] O.M. Kane, J. Appl. Phys. 56 (5) (1984) 1267.
[16] E.M. VanVeldhuizen, F.J. deHoog, D.C. Schram, J. Appl. Phys. 56 (7) (1984) 2047.
[17] V.D. Wisehart, Private Communication, Butler University, 1994.